# ISTITUTO SUPERIORE DI SANITÀ

# The alpha-particle irradiator
# set up at the ISS for radiobiological studies
# on targeted and non-targeted effects

Giuseppe Esposito, Francesca Antonelli, Mauro Belli,
Alessandro Campa, Giustina Simone, Eugenio Sorrentino,
Maria Antonella Tabocchini

*Dipartimento di Tecnologie e Salute*

Istituto Superiore di Sanità
**The alpha-particle irradiator set up at the ISS for radiobiological studies on targeted and non-targeted effects.**
Giuseppe Esposito, Francesca Antonelli, Mauro Belli, Alessandro Campa, Giustina Simone, Eugenio Sorrentino, Maria Antonella Tabocchini
2008, 30 p. Rapporti ISTISAN 08/29

In this paper we describe the alpha-particle irradiator that has been set up at the Istituto Superiore di Sanità (ISS) for controlled exposure of cultured mammalian cells. It can be equipped with two different sources, namely $^{244}$Cm and $^{241}$Am, allowing irradiation at different dose-rates (typically 1-100 mGy/min). The irradiator has dimensions small enough to be inserted into a standard cell culture incubator to perform irradiation of cultured cells in physiological conditions. The dose uniformity is such that the variations in the irradiation area are less than ± 12% of the average dose value on different irradiation areas up to ~25 cm$^2$. Moreover, in the framework of the FP6 Euratom Integrated Project "Non-targeted effects of ionizing radiation (NOTE)", Petri dishes were realized for housing permeable membrane insert(s) to be used in co-culture experiments. Aluminium shields were also realized for half-shield irradiation experiments. The alpha-particle irradiator of the ISS has been successfully used for studying DNA damage, namely double strand breaks (DSB, as measured by the γ-H2AX assay), in directly hit and in bystander primary human fibroblasts.
*Key words*: Alpha-particles, DNA Damage, Bystander effects

Istituto Superiore di Sanità
**L'irradiatore alfa realizzato presso l'ISS per studi radiobiologici sugli effetti "targeted" e "non-targeted".**
Giuseppe Esposito, Francesca Antonelli, Mauro Belli, Alessandro Campa, Giustina Simone, Eugenio Sorrentino, Maria Antonella Tabocchini
2008, 30 p. Rapporti ISTISAN 08/29 (in inglese)

In questo lavoro è descritto l'irradiatore alfa realizzato presso l'Istituto Superiore di Sanità (ISS) per esposizioni di cellule di mammifero in coltura in condizioni controllate. Possono essere utilizzate sia una sorgente di $^{244}$Cm che una di $^{241}$Am, con le quali è possibile effettuare irradiazioni a diversi ratei di dose (typically 1-100 mGy/min). L'irradiatore ha dimensioni sufficientemente contenute da poter essere facilmente collocato all'interno di un incubatore a CO$_2$ standard, il che consente di effettuare irradiazioni di cellule in coltura in condizioni fisiologiche. L'uniformità di dose è tale che le variazioni all'interno della superficie irradiata sono inferiori a ± 12% del valore medio della dose per superfici fino a ~25 cm$^2$. Inoltre, nell'ambito del Progetto Integrato "Non-targeted effects of ionizing radiation (NOTE)", Euratom FP6, sono state realizzate speciali piastre per irradiazione all'interno delle quali possono essere posti degli inserti con base permeabile per esperimenti di co-coltura. Sono stati inoltre realizzati schermi in alluminio che consentono di irradiare solo una frazione della popolazione cellulare. L'irradiatore alfa è stato utilizzato con successo per studiare il danno radioindotto al DNA (in particolare doppie rotture, mediante l'analisi della fosforilazione dell'istone H2AX) in fibroblasti umani primari direttamente irradiati o bystander.
*Parole chiave*: Particelle alfa, Danni al DNA, Effetti bystander

Per informazioni su questo documento scrivere a: giuseppe.esposito@iss.infn.it, antonella.tabocchini@iss.it

Il rapporto è accessibile online dal sito di questo Istituto: www.iss.it.

# TABLE OF CONTENTS

# INTRODUCTION

Alpha-particles represent an important component of population exposure to the natural background radiation, which is largely due to inhalation of radon and its daughters. Due to their relevance for radiation protection, the biological effects of alpha-particles have been extensively studied (see, for instance, Thacker *et al*., 1982; Raju *et al*., 1991; Brooks *et al*., 1994; Hofmann *et al*., 2000; Hofmann *et al*., 2002; Buffler *et al*., 2001; Hall & Hei, 2003; Charles & Harrison, 2007), putting into evidence striking differences between the effects of alpha-particles and those of sparsely ionizing radiation, such as X or γ-rays. There is a large consensus that such differences arise from the spatial (and perhaps temporal) distributions of the energy depositions of the different radiation types. While sparsely ionizing radiation mainly produce single isolated and sparse ionizations, with a substantial component of localized clusters only at the track end of the secondary electrons, for densely ionizing radiation such as alpha-particles, the energy deposition is instead characterized by an almost continuous and well defined track of ionization with clusters at the nanometer level. The diameter of the track, determined by the maximum range of secondary electrons, is dependent on the particle velocity while the ionization density along the track (the Linear Energy Transfer, LET), determined by the energy loss of the particle, is dependent on $(Z_{eff}/\beta)^2$ with $Z_{eff}$ being the effective particle charge and $\beta$ its velocity relative to that of the light.

It has been commonly accepted for many years that biological effects at cellular level, such as cell inactivation, mutation induction and oncogenic transformation, are a direct consequence of the initial damage processing, in particular of the DNA Double Strand Breaks (DSB). Indeed, experimental data indicate that DSB induced by densely ionizing radiation are spatially correlated, more complex (i.e., associated with other lesions) and difficult to repair with respect to those induced by X- or γ-rays (Goodhead, 1994; Rydberg *et al*., 1998; Stenerlow *et al*., 2000; Belli *et al*., 2006).

The central role of DNA damage represented a basic paradigm in radiobiology that has been challenged by a range of evidences observed in the last decade at very low doses. Phenomena such as bystander effects, genomic instability and adaptive response have been called "non-(DNA)-targeted" effects because they do not require direct nuclear exposure by radiation. Briefly, bystander effects are those responses observed in unirradiated cells as a result of receiving signals from irradiated cells; genomic instability describes an increased rate of genetic alterations in the progeny of cells surviving exposure to ionizing radiation; adaptive response is a phenomenon in which resistance to a challenging dose of radiation is established by a small preceding dose (see, for instance, Joiner *et al*., 1996; Mothersill & Seymour, 2001; Mothersill & Seymour, 2004; Morgan, 2003; Kadhim *et al*., 2004).

These phenomena may have important consequences for health risk assessment, in particular they may have implications for the applicability of the Linear No Threshold (LNT) model in extrapolating radiation risk data into the low-dose region; furthermore, implications can also be envisaged for "out of field", or abscopal, effects following diagnostic or therapeutic procedures (Mothersill *et al*., 2004; Prise *et al*., 2005; Mackronis *et al*., 2007).

Beside their relevance for radiation protection purposes, alpha-particles represent an extremely useful tool for investigating bystander effects, especially when the experiments are performed using co-cultures, with irradiated and unirradiated cells sharing the culture medium. In fact, the residual range of alpha-particles is limited enough to allow the study of bystander effects in cells grown into permeable membrane inserts during irradiation of cells attached on the Mylar® bottom of especially designed Petri dishes. Another possibility to study bystander

effects with alpha-particles is by shielding half of the irradiation dish. In this way it is possible to investigate biological effects in unirradiated cells grown in the same dish of, and at various distances from, irradiated cells.

In this paper we describe the alpha-particle irradiator that has been set up at the Istituto Superiore di Sanità (ISS) for controlled exposure of cultured mammalian cells. It represents the evolution of a prototype developed for protracted exposure of cultured cells (Esposito *et al.*, 2006) and can be equipped with two different sources, namely $^{244}$Cm and $^{241}$Am, allowing irradiation at various dose-rates (typically 1-100 mGy/min).

When compared to the already existing alpha-irradiators (see, for instance, Inkret *et al.*, 1990; Goodhead *et al.*, 1991; Cera *et al.*, 1992; Metting *et al.*, 1995; Neti *et al.*, 2004; Wang & Coderre, 2005) the main features of the ISS irradiator are the following:

– It has dimensions small enough to be inserted into a standard cell culture incubator and can be safely used at the atmosphere (98% humidity, 5% $CO_2$) and at the temperature (37°C) inside it; this allows to perform irradiation of cultured cells in physiological conditions, and for relatively long period of time.

– The distance between the source and the sample can be varied in order to further modify the dose-rate and to achieve a dose uniformity such that the variations in the irradiation area are no more than ± 12% of the average dose value on different irradiation surfaces/areas up to ~25 cm$^2$ (56 mm diameter), that is comparable to the area of a commercial T-25 flask for cell culture.

Moreover, in the framework of the FP6 Euratom Integrated Project "Non-targeted effects of ionizing radiation (NOTE)", Petri dishes were realized for housing permeable membrane insert(s) that exactly reproduce the geometry of commercial Cell Culture Insert Companion Plates. Aluminum shields were also realized for half-shield irradiation experiments.

The alpha-particle irradiator of the ISS here described has been successfully used for studying DNA damage, namely Double Strand Breaks (DSB, as measured by the γ-H2AX assay), in directly hit and in bystander primary human fibroblasts.

# 1. MATERIALS AND METHODS

## 1.1. Design and construction of the alpha-irradiator

### 1.1.1. The alpha-sources

The irradiator can be equipped with two different alpha-sources, namely a [244]Cm source and an [241]Am source, with total activities of about 112 kBq and 3685 kBq respectively (at July 2008).

The [244]Cm source decay yields the highest alpha-particle energy (5805 keV) among the commonly available transuranic emitters, although its half-life (18.10 y) is not very long. [244]Cm decays to [240]Pu, a long half-life alpha-emitter (6563 y) with no significant interfering beta emissions or conversion electrons. An extended source of 20-mm-diameter emitting surface was especially manufactured by Isotope Products Laboratory, USA. The emitting material, made of electrodeposited and diffusion-bonded [244]Cm oxide, is protected by a very thin gold coating of 0.026 μm.

The [241]Am source decay yields alpha-particles with energy of about 5500 keV and its half-life is 432.2 y. [241]Am decays to [237]Np, itself a long half-life alpha-emitter (about $2 \times 10^6$ y) with no significant interfering beta emissions or conversion electrons. Moreover, [241]Am is one of the alpha-emitters with higher total activity among those available on the market and this made it complementary to the [244]Cm source. An extended source of 11.1-mm-diameter emitting surface was especially manufactured by Isotope Products Laboratory, USA. In this case, the emitting material, made of solid metal [241]Am foil, is protected by a thin gold coating of 1.61 μm.

As a matter of fact, γ-rays with different energies and intensities are released during the decay of both [244]Cm and [241]Am; however the γ-ray doses calculated by GEANT4 (http://geant4.web.cern.ch/geant4/) at the cell entrance are negligible compared to the alpha-particle doses, and this is crucial for bystander experiments (for details see Appendix A).

The required uniformity in distribution of alpha-particle fluence on the sample has been obtained by a suitable source-to-sample distance. However, increasing this distance decreases fluence and also increases energy degradation of the alpha-particles due to the gas used to fill the chamber in order to balance the outside pressure (see below). Although a low-atomic-number gas, such as helium, was used, this still causes some energy degradation. The source-to-target distance of 59 mm was chosen for acceptable uniformity of the radiation field with minimum energy degradation.

The values of energy, LET, dose-rate and the residual range of the alpha-particles from the two sources in such conditions are reported in Table 1.

**Table 1. Characteristics of the alpha-sources used at the ISS**

| Alpha-source | Energy (incident to the cells) | LET (incident to the cells) | Dose-rate | Residual range |
|---|---|---|---|---|
| [244]Cm | 3.1 MeV | 122 keV/μm | ~2.7 mGy/min (~0.16 Gy/h) | ~19 mm |
| [241]Am | 3.0 MeV | 125 keV/μm | ~84 mGy/min (~5 Gy/h) | ~18 mm |

### 1.1.2. The irradiation chamber and the especially designed Petri dishes

Figure 1 shows a sketch of the irradiation chamber. The body of the irradiation chamber is made of a stainless steel cylinder, 240 mm in diameter and 197 mm high, with bottom and top closed by flanges of the same stainless steel. The top flange has a hole where the especially designed Petri dish (see below) can be inserted. The Petri dish also acts as a seal for the chamber since its Mylar® bottom separates the inner helium gas from the outside where the cells are kept at atmospheric pressure. This solution avoids the presence of an additional foil as an exit window, present in some other alpha-irradiators, and the consequent air layer between this window and the Petri dish bottom.

On the top flange, besides the Petri dish, there is an Ion-Implanted-Silicon charged-particle Detector (IISD, Ortec model BU-020-450-AS), used to monitor particle energy during cell irradiation. This is useful for verifying the absence of significant air contamination in the helium atmosphere inside the chamber.
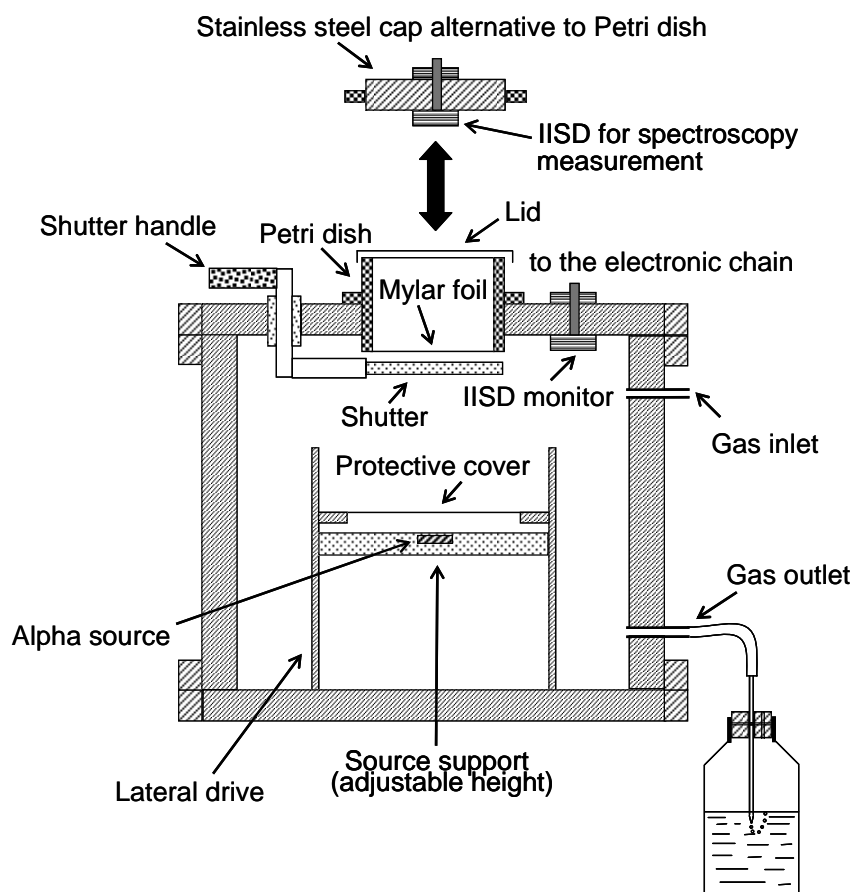


**Figure 1. Sketch of the irradiation chamber**

The alpha-source is housed in a cylindrical polyvinyl chloride holder placed in the central position of the chamber, which can be adjusted at the desired height. An additional protective

cover, made of a Mylar® foil 6 μm thick (for the [244]Cm source) or 0.7 μm thick (for the [241]Am source), is placed over the source holder. This has the scope to prevent contamination or soiling of the source surface from unlikely, but possible, spillage of culture medium in case of damage or breakdown of the Mylar® bottom of the Petri dish. A shutter, consisting of a shaft sliding through a vacuum-tight support, having a circular stainless plate of suitable diameter, can be manually driven from outside the chamber to start and stop irradiation.

The chamber can be filled with helium gas in order to reduce energy loss of alpha-particles emitted by the source. To keep high-purity helium atmosphere inside the chamber for the needed period of time, a continuous gas flow is provided through inlet and outlet flanges equipped with tubes and valves. In order to avoid deformation of the Mylar® foil in the Petri dish, the inside pressure is kept very close to the external one. This is accomplished by a combined use of a precision adjustable valve at the inlet side, and of a bubbler device at the outlet side. The bubbler tip was dipped into water for a few mm in order to allows a very small pressure differential (typically 50 Pa (0.38 mmHg) corresponding to an overpressure of about 0.05% respect to the outside pressure) at a flow rate of about 100 $cm^3$ $min^{-1}$. Under these conditions there are no visible deformations in the Mylar® foil. A flange with a quartz window allows visual inspection of the chamber interior during operation.

The standard Petri dish, designed for irradiation of cultured cells, is made of stainless steel, with a 6 μm-thick (for [244]Cm source) or 3 μm-thick (for [241]Am source) Mylar® bottom having 56 mm inner diameter (area of 24.6 $cm^2$, i.e. comparable to a commercial T-25 flask), where cells can grow as monolayer (Figure 2 A).

For bystander effect studies, ~1.2 mm thick Al shields were realized for shielding half the Petri dish. Moreover, stainless steel Petri dishes were especially designed for housing permeable membrane inserts. They exactly reproduce the geometry of commercial Cell Culture Insert Companion Plates. Stainless steel companion dishes with three independent irradiation vessels (irradiation area of 3.8 $cm^2$ each) or one vessel only (irradiation area of 9.6 $cm^2$) were constructed, able to housing inserts of 0.9 $cm^2$ or 4.2 $cm^2$ growth area, respectively (Figure 2 B and C).



**Figure 2. Stainless steel Petri dish (A) designed for the alpha-particle irradiator (~25 $cm^2$ useful area), able to allocate the companion dishes B or C for experiments with inserts**

Adaptors were realized for maintaining the distance of 0.9 mm from the insert base to the Mylar® bottom of the dish; such distance can be increased, if requested.

A stainless steel cap is available to substitute for the Petri dish. It is equipped at its centre with a vacuum-tight (plug) holder for the ion-implanted-silicon charged-particle detector, with the sensitive area positioned at the same distance to the source as the Petri dish bottom. This cap has a two-fold function: it is used for spectroscopy measurement of the particles impinging on the cells (in this case a Mylar® foil is placed in front of the detector to simulate the Petri dish Mylar® bottom), and it serves as a seal to speed-up air evacuation from the chamber at the beginning of operation (see Results).

The overall size of the chamber is 24 cm (diameter) × 20 cm (height), small enough to be easily positioned into a cell culture incubator of usual size (Figure 3).



**Figure 3. The alpha-irradiator placed into a standard $CO_2$ incubator**

## 1.2. Spectrometry and dosimetry

The absorbed dose rate and uniformity at the sample position have been derived from alpha-particle energy distribution (which gives LET distribution) and particle fluence rate evaluated by calculations, and then checked by measurements made at the sample position. Since measurements confirmed the results of calculations, this method was also used to evaluate the dose rate at the cell mid-plane and, therefore, the irradiation time needed to reach the desired total dose. The following basic expression relating the dose $D$, the fluence $F$ and the LET $L$ was used:

$$D[\text{Gy}] = 1.6 \cdot 10^{-9} \, \rho^{-1}[\text{g}^{-1} \text{ cm}^3] \cdot F[\text{cm}^{-2}] \cdot L[\text{keV } \mu\text{m}^{-1}] \qquad [1]$$

where $\rho$ is the density of the sample. For this calculation, it was assumed a cell composition equal to that of the MS20 tissue substitute [International Commission Radiation Units and Measurements 1993], where $\rho = 1$ g cm$^{-3}$.

Calculations have been performed to evaluate the energy distributions in any point of the irradiated sample. Validation of the procedure was accomplished by comparison with experimental results obtained for a defined geometry.

Average particle fluence rate and uniformity at the sample position were also calculated as described in Appendix B. Briefly, particle fluence rate $\phi(x)$ as a function of distance $x$ from the centre of the sample was calculated using the relationship:

$$\phi(x) = \frac{A}{4\pi^2 R^2} \int_0^{2\pi} \left( \int_0^R \frac{r \cdot h}{(h^2 + x^2 + r^2 - 2 \cdot r \cdot x \cdot cos\alpha)^{3/2}} \, dr \right) d\alpha \qquad [2]$$

where A is the activity of the source, $r$ is the distance of an arbitrary source point from the source centre, $h$ is the source-to-sample distance, $x$ is the distance of the considered sample point from the sample centre, $X$ is the sample radius and $\alpha$ is the angle between $x$ and the projected $r$. The average particle fluence rate is given by:

$$\overline{\phi} = \frac{\int_0^X 2 \cdot \pi \cdot \phi(x) \cdot x \cdot dx}{\pi \cdot X^2} \qquad [3]$$

The fluence rate uniformity was evaluated by the ratios of the maximum and minimum fluence rate to its average value:

$$\phi(x = 0) / \overline{\phi} \ and \ \phi(x = X) / \overline{\phi} \qquad [4]$$

The energy distribution at the position of the cell monolayer was simulated using the Monte Carlo simulation program TRIM (Ziegler *et al.,* 1985), which follows the history of a number of alpha-particles emitted by the source (details are reported in Appendix C).

The energy spectrum also was measured at the position of the cell monolayer by means of an IISD, housed in a stainless steel cap inserted instead of the Petri dish, as described in Sect. 2.1.2. The detector was connected to an electronic chain implemented by NIM-modules that includes a preamplifier with its bias supply, a linear amplifier and a MultiChannel Analyzer (MCA). Acquisition of spectra was performed with a personal computer interfaced with the MCA and equipped with management software (MAESTRO-32 by ORTEC).

Particle fluence rate and its uniformity at the sample position were measured by CR39 plastic track detectors. CR39 discs, 56 mm diameter and 1 mm thick, were placed at the sample position in the stainless steel Petri dish, in contact with its Mylar® bottom and were irradiated for an appropriate time to obtain a good count statistics with no or minimal pit overlapping.

Three independent irradiations were performed. After irradiation, detectors were etched in 6.25 N NaOH at 70°C for 4 hours and the numbers of tracks per unit area were counted using an optical microscope equipped with a CCD camera.

In order to obtain particle fluence rate as a function of distance from the centre of the circular irradiated area, several fields were counted at different positions along two perpendicular diameters and those at the same distance from the centre were averaged. Then the average, weighted with this distance, was calculated to determine the mean value on the overall irradiated area. Uniformity was evaluated as the ratios of the values measured at the edge and at the centre to the average value.

# 2. RESULTS AND DISCUSSION

## 2.1. Operation

The alpha-particle irradiator has been designed to perform exposures of cultured mammalian cells typically at 1-100 mGy/min, depending on the alpha-source used, with a dose uniformity on the sample such that the variations in the irradiation area are no more than ± 12%. To this purpose, step by step calculations were carried out to find the source-to-sample distance, $h$, that satisfies both requirements for dose-rate and uniformity. When the distance $h$ between the alpha source and the sample was 59 mm, average dose rates of 2.7 mGy/min and 84 mGy/min, with the required dose uniformity were found for $^{244}$Cm and $^{241}$Am sources respectively.

To start operation, the chamber cap, housing the IISD to be used for spectrometry measurements, is installed instead of the Petri dish. The chamber is then inserted in a cell culture incubator operating at 37°C with an atmosphere of air and 5% $CO_2$. After a time sufficient for temperature equilibration, the chamber is first evacuated by means of a turbomolecular pump connected to the outlet pipe, and then filled with helium gas (99.9995% purity). In this arrangement the substitution of air with helium is facilitated due to the absence of a Mylar® exit window that otherwise would not survive air evacuation by the turbomolecular pump. After complete filling with helium, the chamber is flushed with the same gas, at a flow rate kept at about 100 cm$^3$ min$^{-1}$ during spectroscopy measurements.

This procedure is also used before inserting the Petri dish with the cells to be irradiated. In this case, after filling the chamber with helium gas, the metal cap is quickly removed and the Petri dish is placed instead of it, increasing the helium flow to about 200 cm$^3$ min$^{-1}$ to wash out residual air inside the chamber. As soon as the IISD monitor next to the Petri dish indicated that the energy spectrum was stable, with the peak corresponding to the expected value, according to the calculations, the helium flow is adjusted at its normal operating value. The time needed for equilibrating the chamber was typically found to be 5-10 min.

## 2.2. Spectrometry

The experimental energy spectrum at the cell entrance was compared with the simulated spectrum at the position of the actual detector, considering its sensitive area. Table 2 reports the value relative to the two alpha-sources.

The difference between simulated and experimental average values of alpha-particle energies is ≤36 keV, which is within the energy resolution of the spectrometric system. This fairly good agreement indicates that this simulation evaluated the energy distribution with a reasonable approximation.

**Table 2. Experimental and simulated average energy values for the two alpha-sources**

| Alpha-source | Experimental energy value (keV) | Simulated energy value (keV) |
|---|---|---|
| $^{244}$Cm | 3301 | 3265 |
| $^{241}$Am | 3168 | 3159 |

Simulation was therefore used to evaluate the LET distribution over the area of the Petri dish, for both $^{244}$Cm and $^{241}$Am sources. Figure 4 shows the obtained LET values evaluated from the energy distribution using the ICRU tables (International Commission on Radiation Units and Measurements, 1993) and performing a linear interpolation. The average value $L_{ave}$ is 122 keV $\mu$m$^{-1}$ for $^{244}$Cm and 124.6 keV $\mu$m$^{-1}$ for $^{241}$Am, with *FWHM/$L_{ave}$* ratio of 0.07 and 0.06 respectively. Being the LET variations quite limited, the use of $L_{ave}$ for dose calculation in any point of the sample surface, and evaluation according to Eq. [1], can be considered as an acceptable approximation.
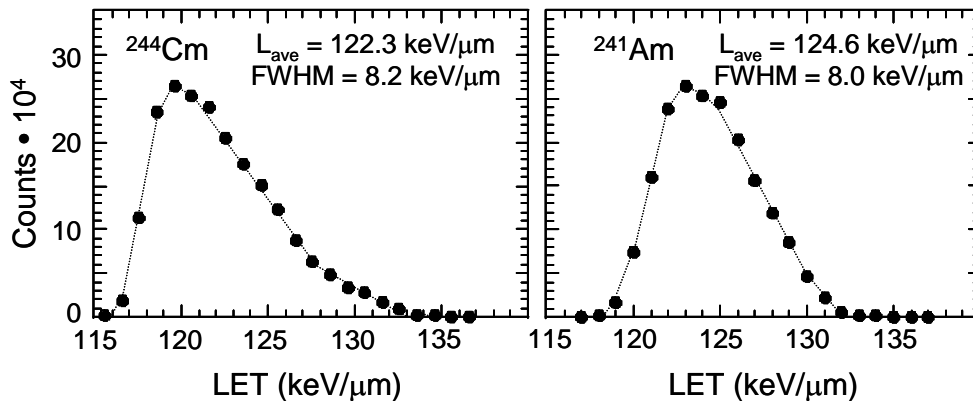


**Figure 4. Distributions of LET values at the cell entrance for $^{244}$Cm and $^{241}$Am sources, calculated from the simulated energy distributions over the Petri dish area (the light dotted lines are guides for the eye)**

## 2.3. Fluence rate and dose rate

CR39 plastic detectors have been used to measure the fluence rate and the distribution of particles emitted by both $^{244}$Cm and $^{241}$Am sources at the sample position, as described in *Materials and Method*.

To evaluate the fluence distribution, five different radial positions, from centre to edge, were considered. For each of them, the number of pits included in a field of $5.6 \times 10^{-4}$ cm$^2$ area was counted. This procedure was repeated four times at four perpendicular radii and the numbers of pits in the four fields corresponding to the same radial position were summed up.

Figure 5 shows two typical fields of the etched tracks obtained after about 600 s and 22 s exposure (to obtain a comparable number of pits) to $^{244}$Cm and $^{241}$Am respectively at the centre and at the edge of the detector.

The total number of pits counted per position was not less than 90 so that about 400 pits for each radial position were counted.
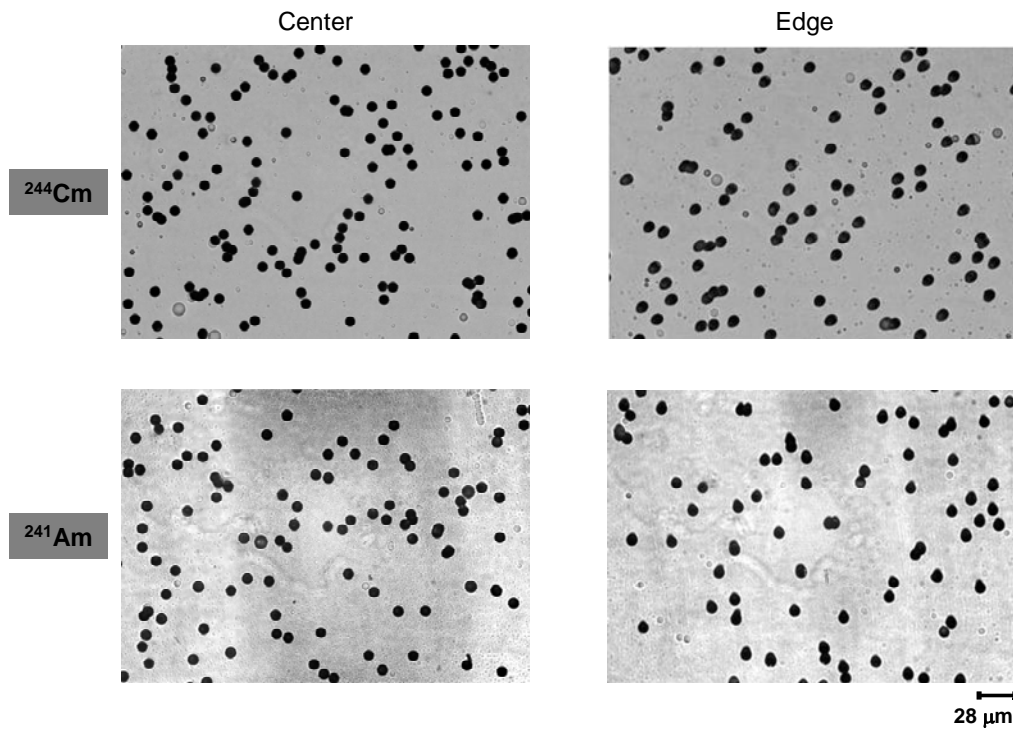
| Center | Edge |
| --- | --- |



**²⁴⁴Cm**

**²⁴¹Am**

28 μm

**Figure 5. Photographs (magnification 40x) of the etched tracks in CR39 discs**
**for ²⁴⁴Cm and ²⁴¹Am, showing typical fields at the centre and at edge of the Petri dish**

For ²⁴⁴Cm source the average fluence rate $\overline{\phi}$ was (224±3) cm⁻² s⁻¹ and the fluence rate variation was determined to be:

$$\frac{\phi_{center}}{\overline{\phi}} = 1.15 \pm 0.03 \quad \text{and} \quad \frac{\phi_{edge}}{\overline{\phi}} = 0.89 \pm 0.02 \,.$$

For ²⁴¹Am source the average fluence rate was (6925±169) cm⁻² s⁻¹ and the fluence rate variation was determined to be:

$$\frac{\phi_{center}}{\overline{\phi}} = 1.15 \pm 0.04 \quad \text{and} \quad \frac{\phi_{edge}}{\overline{\phi}} = 0.89 \pm 0.03 \,.$$

These values derived from measurements with CR39 detectors can be compared with the calculations carried out solving numerically the equations [2] and [3].

Table 3 summarizes the results of these calculations in terms of fluence rate variations for both ²⁴⁴Cm and ²⁴¹Am sources. It can be seen that there is a good agreement between experimental and calculated values, confirming that the calculation procedure is reliable.

**Table 3. Fluence (φ) and dose (D) variations evaluated by the ratios between their values**
**at the centre and at the edge of the biological sample and their average values**

| Alpha-source | $\phi_{centre}$ / $\phi_{ave}$ | $\phi_{edge}$ / $\phi_{ave}$ | $D_{centre}$ / $D_{ave}$ | $D_{edge}$ / $D_{ave}$ |
| --- | --- | --- | --- | --- |
| ²⁴⁴Cm | 1.15 | 0.89 | 1.12 | 0.92 |
| ²⁴¹Am | 1.14 | 0.89 | 1.12 | 0.91 |

## 2.4. Time stability

Long-term stability of the exposure conditions is an important requirement for protracted experiments. To check the stability of the system, two irradiations with $^{244}$Cm were performed for up to 16 days. The energy spectra were recorded at the beginning and at the end of the scheduled time, without significant variation (*i.e.*, they were within the overall system precision). Also, the effects of the changes in the atmospheric pressure were experimentally monitored, since they affect the helium gas density and therefore the energy loss of the alpha-particles. Energy spectra and values were measured during conditions of medium pressure (corresponding to the standard pressure of 760 mmHg). In addition, energy spectra were recorded over a period of many months when situations of both high (765 mmHg) and low (756 mmHg) atmospheric pressure occurred. The measured average energy changed accordingly from 3301 keV (medium) to 3247 keV (high) and to 3327 keV (low) corresponding to LET variations from 120.4 keV $\mu$m$^{-1}$ to 121.7 keV $\mu$m$^{-1}$ and 119.8 keV $\mu$m$^{-1}$, respectively. It appears that these changes, resulting in dose variations less than 2%, are negligible for the application which the irradiator was devoted to.

Helium consumption is such that there is no need to change the gas tank for irradiations lasting up to 16 days.

## 2.5. Direct damage and bystander effect experiments in cultured mammalian cells

The alpha-particle irradiator was used to perform experiments on DNA damage, (namely double strand breaks, DSB, as measured by the γ-H2AX assay) induced directly or as a result of bystander mechanisms in AG1522 primary human fibroblasts. Details of the experimental procedure are reported elsewhere (Antonelli *et al*., 2005). Here we only mention that DSB are visualized in the cell nucleus as fluorescent foci using antibodies against the phosphorylated form of histone H2AX (γ-H2AX), that rapidly occurs after DNA DSB induction.

For direct damage experiments as well as for the experiments aimed at investigating "medium mediated" bystander effects, 14/18 h before irradiation the cells were seeded into the stainless steel Petri dishes and left them to attach at the Mylar® base of the dish. The Petri dishes were then inserted and kept into the top flange hole of the irradiator with the shutter closed for 5-10 min, i.e. the time needed for equilibrating the helium pressure into the irradiation chamber, before being irradiated.

### 2.5.1. Direct damage: DNA DSB induction and repair experiments

For the experiments on DNA damage induction, the samples were exposed at 4°C (into a fridge) to the $^{231}$Am alpha-particles for different times, corresponding to the requested doses ranging from 0.1 to 1.0 Gy. The results obtained, reported in Figure 6, show a linear relationship between the number of induced foci and the dose.

Further experiments were performed to analyze the repair kinetics up to 4 hours from irradiation. Cells were irradiated with 0.5 Gy at 4°C or at 37°C (into the incubator) and then incubated for different times at 37°C.
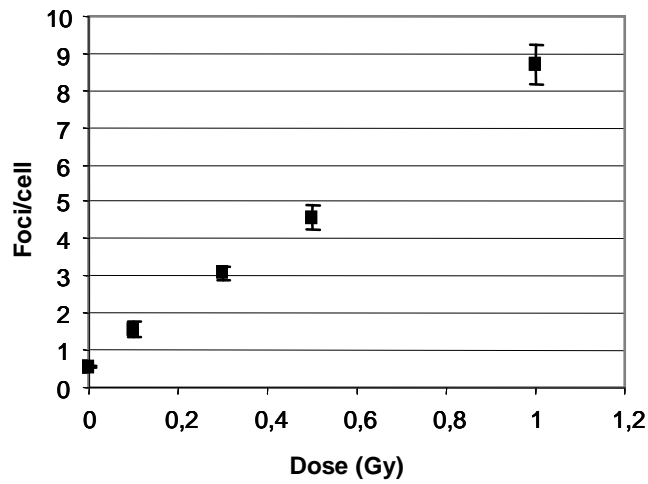
**Figure 6. Average number of foci/cell induced as a function of the alpha-particle dose in AG11522 human fibroblasts**

As shown in Figure 7 a reduction of the number of foci is observed with increasing incubation time, and the kinetics is independent on the irradiation temperature.
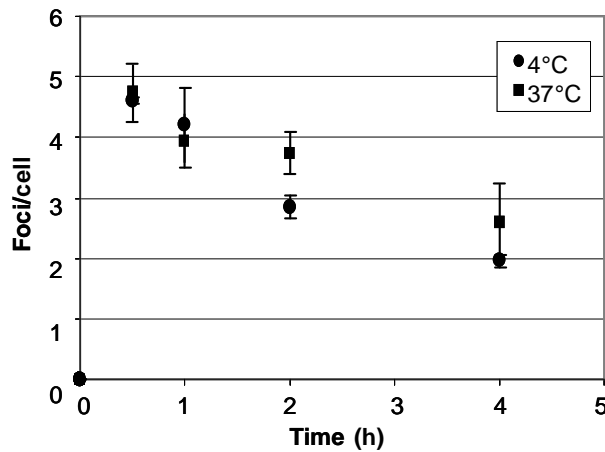


**Figure 7. Foci repair kinetics after 0.5 Gy alpha-particles**

## 2.5.2. DNA DSB induction in bystander cells

Different approaches were used for bystander effects studies, namely the co-culture of irradiated cells with unirradiated cells grown in insert and the partial shielding of the Petri dish with irradiated and unirradiated cells growing on the same Mylar® foil (Figure 8).
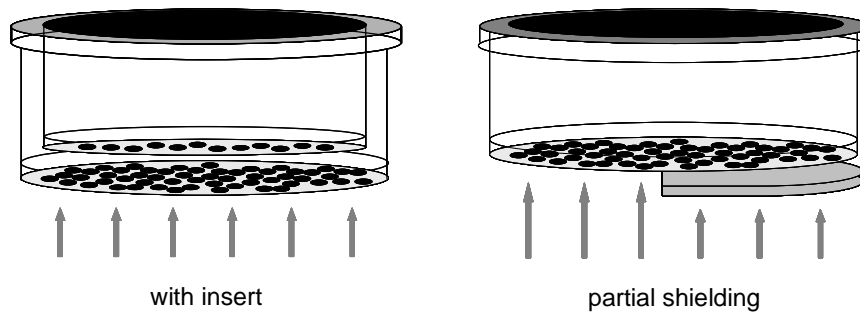
**Figure 8. Sketch of the different co-culture approaches used for bystander experiments**

As already mentioned, companion stainless steel Petri dishes were especially designed for housing permeable membrane insert(s) (see Figure 2 B and C) that exactly reproduce the geometry of commercial Cell Culture Insert Companion Plates. Bystander experiments on DNA damage were carried out using the dishes with three independent irradiation vessels (irradiation area of 3.8 cm$^2$ each), able to housing three inserts of 0.9 cm$^2$ cell growth area. Due to the limited residual range of alpha-particles, only cells growing on the bottom of the Mylar® based Petri dish were irradiated and bystander effects were studied in co-cultured cells placed ~1 mm apart into the permeable membrane inserts. For these studies the irradiator has been located into the CO$_2$ incubator at 37°C, allowing irradiation and post-irradiation incubation in the presence of irradiated cells without moving the samples. After irradiation with a dose of 0.5 Gy, the shutter was closed and the cells in inserts maintained for different times sharing medium with irradiated cells.

Figure 9 shows the percentage of bystander cells with γ-H2AX foci after different co-culture time (up to 2h) with cells irradiated with alpha-particles from the [231]Am source.
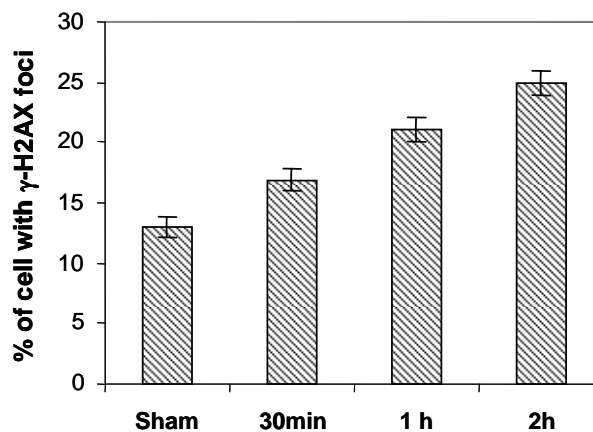


**Figure 9. Effect of the time of co-culturing of targeted and bystander cells on the induction of γ-H2AX foci in bystander cells. Targeted cells were irradiated with 0.5 Gy alpha-particles**

A slight increase in the number of positive cells with respect to the sham control is visible at 30 min of co-culture, which becomes more evident after 1 and 2 hours of co-culture (Alloni *et al.*, 2008). In this configuration, targeted and bystander cells are not in contact, so that communication between irradiated and unirradiated cells by gap-junctions is prevented and only the effect of

signalling molecules released in the culture medium is responsible for the observed effect (*i.e.*, the so-called "medium-mediated bystander effect"). The degree of this response seems to increase, under the conditions considered herein, with the co-culture time. The results of partial shielding experiments are reported in Figure 10.
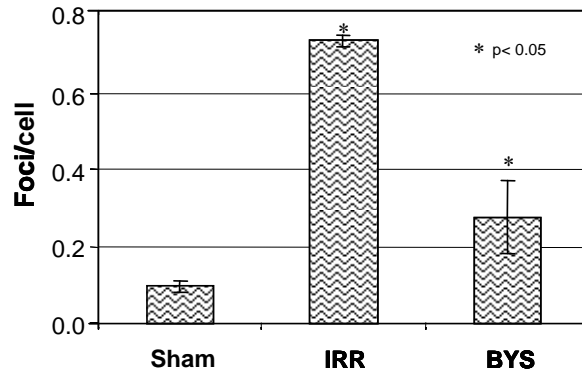


**Figure 10. Number of foci/cell in AG1522 fibroblasts unirradiated (CN), 0.5 Gy irradiated (IRR) and bystander (BYS), after 22 h of incubation time at 37°C from irradiation**

In this configuration, as already mentioned, the cells growing on the Mylar® base of the Petri dish were half irradiated with alpha-particles from the $^{244}$Cm source, by positioning an Al shield immediately below the dish. In this way, zones of bystander and hit cells all in the same plane can be obtained to evaluate the contribution of the medium mediated bystander effect only.

Our results show that, after 22 h of cell incubation at 37°C from irradiation, the number of foci/cell in irradiated cells ($0.74 \pm 0.02$) is increased by a factor of about 8 with respect to sham-irradiated cells ($0.095 \pm 0.020$). In bystander cells, the number of foci/cell ($0.28 \pm 0.10$) is much lower than that observed in directly hit cells but still significantly higher than in the sham-irradiated cells by a factor of about 3.

# CONCLUSIONS

The alpha-particle irradiator here described provides a useful facility for irradiation of cultured mammalian cells with alpha-particles at different dose rate. It has been successfully used for benchmark radiobiological studies on DNA damage, namely DSB (as measured by the γ-H2AX assay), in directly hit and in bystander primary human fibroblasts and it is currently used to perform a systematic study on bystander effects under controlled conditions in the framework of the NOTE Project (FP6-EURATOM).

At the present the alpha-irradiator can be equipped with two different sources. The alpha-emitting radionuclide [244]Cm, has the advantage of giving particles with an energy (and therefore a residual range) slightly higher than that given by other commonly available transuranic emitters, including [238]Pu that is used in most of the existing alpha-irradiators. This feature ensures a better approximation to track-segment irradiation conditions, and makes the experimental results less dependent on the possible presence of cells not perfectly flattened and attached to the Mylar® substrate. The [241]Am source has a total activity thirty times higher than that of the [244]Cm source. This feature allows us to carry out several bystander effect studies minimizing the irradiation time.

The limited size of the irradiation chamber allows its insertion into commercially available cell culture incubators, where temperature and air/$CO_2$ atmosphere are well controlled, avoiding use of "*ad hoc*" and separate devices to these purposes. Detailed spectroscopic and dosimetric characterization of the irradiator as reported here is important when comparing biological results obtained by different laboratories. In the geometry described in this paper (*i.e.* source-to-sample distance = 59 mm) a Petri dish of 25 cm$^2$ area can be irradiated with average dose rates of 2.7 mGy/min and 84 mGy/min and with spatial variations in dose rate of less then ± 12% with respect to this average value for [244]Cm and [241]Am sources, respectively. This uniformity is acceptable for many radiobiological experiments requiring irradiation of mammalian cells with charged particles. It is possible to increase the average dose rate, without changing this uniformity, making small changes in the irradiator, for example reducing both the irradiation area and the source-to-sample distance. Otherwise, if necessary, irradiation uniformity could be enhanced by using a smaller Petri dish or, alternatively, by increasing the source-to-sample distance if a lower dose rate can be accepted.

# REFERENCES

Alloni D, Antonelli F, Ballarini F, Belli M, Bertolotti A, Campa A, Dini V, D'Ercole L, Esposito G, Facoetti A, Friedland W, Giovannini C, Grande S, Guidoni L, Liotta M, Lisciandro F, Luciani AM, Mantovani L, Mariotti L, Molinelli S, Nano R, Ottolenghi A, Palma A, Paretzke HG, Pasi F, Raffaele L, Rosi A, Sapora O, Scannicchio D, Simone G, Sorrentino E, Tabocchini MA, Viti V. Charged particle effects: experimental and theoretical studies on the mechanisms underlying the induction of molecular and cellular damage and the modulation of intercellular signalling. *Il Nuovo Cimento C* 2008;1:21-38.

Antonelli F, Belli M, Cuttone G, Dini V, Esposito G, Simone G, Sorrentino E, Tabocchini MA. Induction and repair of DNA double strand breaks in human cells: dephosphorylation of histone H2AX and hits inhibition by calyculin A. *Radiat Res* 2005;164:514-17.

Belli M Cherubini R, Dalla Vecchia M, Dini V, Esposito G, Moschini G, Sapora O, Simone G and Tabocchini MA. DNA fragmentation in V79 cells irradiated with light ions as measured by PFGE. I. Experimental results. *Int J Radiat Biol* 2006;78:475-82.

Bouffler SD, Haines JW, Edwards AA, Harrison JD, Cox R. Lack of detectable transmissible chromosomal instability after in vivo or in vitro exposure of mouse bone marrow cells to $^{224}$Ra alpha particles. *Radiat Res* 2001;155(2):345-52.

Brooks AL, Khan MA, Duncan A, Buschbom RL, Jostes RF, Cross FT. Effectiveness of radon relative to acute 60Co gamma-rays for induction of micronuclei in vitro and in vivo. *Int J Radiat Biol* 1994;66(6):801-8.

Cera F, Cherubini R, Galeazzi G, Haque AMI, Moschini G, Tiveron P. Cell irradiation system with alpha sources. In: *Annual Report 1992*. Legnaro: LNL; 1993. (LNL-INFN (REP)-72/93). p. 89-90

Charles MW, Harrison JD. Hot particle dosimetry and radiobiology – past and present. *Radiol Prot* 2007;(3A):A97-109.

Esposito G, Belli M, Simone G, Sorrentino E, Tabocchni MA. A $^{244}$Cm irradiator for protracted exposure of cultured mammalian cells with alpha particles. *Health Physics* 2006;90:66-73.

Goodhead DT. Initial events in the cellular effects of ionising radiation: Clustered damage in DNA. *Int J Radiat Biol* 1994;65:7-17.

Goodhead DT, Bance DA, Stretch A, Wilkinson RE. A versatile plutonium–238 irradiator for radiobiological studies with alpha–particles. *Int J Radiat Biol* 1991;59:195-210.

Hall EJ, Hei TK. Genomic instability and bystander effects induced by high-LET radiation. *Oncogene* 2003;22:7034-42.

Hofmann W, Crawford-Brown DJ, Fakir H, Caswell RS. Energy deposition, cellular radiation effects and lung cancer risk by radon progeny alpha particles. *Radiat Prot Dosimetry* 2002;99(1-4):453-6.

Hofmann W, Ménache MG, Crawford-Brown DJ, Caswell RS, Karam LR. Modelling energy deposition and cellular radiation effects in human bronchial epithelium by radon progeny alpha particles. *Health Phys* 2000;78(4):377-93.

Inkret WC, Eisen Y, Harvey WF, Koehler AM, Raju MR. Radiobiology of alpha particles. I. Exposure System and dosimetry. *Radiat Res* 1990;123:304-10.

International Commission on Radiation Units and Measurements. *Stopping powers and ranges for protons and alpha particles*. Bethesda, MD: ICRU; 1993 (ICRU Report 49).

Joiner MC, Lambin P, Malaise EP, Robson T, Arrand JE, Skov KA, Marples B. Hypersensitivity to very-low single radiation doses: its relationship to the adaptive response and induced radioresistance. *Mutat Res* 1996;358(2):171-83.

Kadim MA, Moore SR, Goodwin EH. Interrelationships amongst radiation-induced genomic instability, bystander effects and the adaptive response. *Mutat Res* 2004;568:21-32.

Mackonis EC, Suchowerska N, Zhang M, Ebert M, McKenzie DR, Jackson M. Cellular response to modulated radiation fields. *Phys Med Biol* 2007;52:5469-82.

Metting NF, Koehler AM, Nagasawa H, Nelson JM, Little JB. Design of a benchtop alpha particle irradiator. *Health Phys* 1995;68:710-5.

Mothersill CE, Moriarty MJ, Seymour CB. Radiotherapy and the potential exploitation of bystander effects. *Int J Radiat Oncol Biol Phys* 2004;58(2):575-9.

Mothersill C, Symour C. Radiation induced bystander effects: past history and future directions. *Radiat Res* 2001;155:759-67.

Mothersill C, Symour C. Radiation induced bystander effects and adaptive responses – the yin and yang of low dose radiobiology? *Mutat Res* 2004;168:121-8.

Morgan WF. Non-targeted and delayed effects of exposure to ionizing radiation: I. Radiation-induced genomic instability and bystander effects *in vitro*. *Radiat Res* 2003;159:567-80.

Neti PVS, de Toledo SM, Perumal V, Azzam, Howell RW. A multi-port low fluence alpha-particle irradiator: fabrication, testing and benckmark radiobiological studies. *Radiat Res* 2004;161:732-8.

Prise KM, Schettino G, Folkard M, Held KD. New insights on cell death from radiation exposure. *Lancet Oncol* 2005;6(7):520-8.

Raju MR, Eisen Y, Carpenter S, Inkret WC. Radiobiology of alpha particles. III. Cell inactivation by alpha particle traversals of the cell nucleus. *Radiat Res* 1991;128:204-9.

Rydberg B, Lobrich M, Cooper PK. Repair of clustered DNA damage caused by high LET radiation in human fibroblasts. *Phys Med* 1998;14 Suppl 1:24-8.

Stenerlöw B, Höglund E, Carlsson J, Blomquist E. Rejoining of DNA fragments produced by radiations of different linear energy transfer. *Int J Radiat Biol* 2000;76(4):549-57.

Tapio S, Jacob V. Radioadaptive response revisited. *Radiat Environ Biophys* 2007;46:1-12.

Thacker J, Stretch A, Goodhead DT. The mutagenicity of alpha particles from Plutonium–238. *Radiat Res* 1982;92:343-52.

Ziegler JF, Biersack JP, Littmark U. *The stopping and range of ions in solids*. New York: Pergamon Press; 1985.

Wang R, Coderre JA. A bystander effect in alpha-particle irradiations of human prostate tumor cells. *Radiat Res* 2005;164:711-22.

# APPENDIX A

**Fluence and dose rate of photons released by $^{244}$Cm and $^{241}$Am decay**

Gamma-rays and X-rays are released during the alpha-emitters decay as [244]Cm and [241]Am. The energy and intensity of these photons can be found in tables in the NUDAT retrieval program made available on the Internet by Brookhaven National Laboratory (http://www.nndc.bnl.gov/nudat2/indx_dec.jsp). Specifically the emission probability of photons with energy of 14.3 keV for [244]Cm is about 0.084, while the emission probabilities of all other emitted photons are negligible with respect to these ones. Analogously photons with energies of 13.9 keV, 26.3 keV and 59.5 keV are released for [241]Am with emission probabilities of 0.37, 0.024 and 0.359 respectively. All other photons are negligible relative to these three. The average photon dose rate at the cell entrance has been calculated using this equation:

$$\frac{dD}{dt}(Gy \cdot s^{-1}) = 1.6 \cdot 10^{-13} \cdot \sum_i \left[ \frac{\mu_{en}(E_i)}{\rho}(cm^2 \cdot g^{-1}) \cdot E_i(keV) \cdot \phi(E_i)(cm^{-2} \cdot s^{-1}) \right]$$

where $\mu_{en}/\rho$ is the photon mass energy absorption coefficient in water,
$E_i$ is the photon energy and $\phi$ is the average photon fluence rate at the cell entrance.

The photon mass energy absorption coefficients for the different energy were obtained by NIST web site (http://physics.nist.gov/PhysRefData/XrayMassCoef/tab4.html).

The photon attenuation in different materials traversed was calculated by the Monte Carlo simulation program GEANT4 in the unidimensional case.

The average fluence and dose rates at the sample position for the photons released during the [244]Cm and [241]Am decays are reported in Table A1.

**Table A1. Calculated values for fluence and dose rate of the [244]Cm and [241]Am photons**

| Emitter | Energy (keV) | Average incident fluence rate (cm$^{-2}$ s$^{-1}$) | Average incident dose rate (Gy min$^{-1}$) |
|---------|--------------|----------------------------------------------------|--------------------------------------------|
| [244]Cm | 14.3 | $1.13 \times 10^1$ | $2.48 \times 10^{-9}$ |
| [241]Am | 13.9 | $1.56 \times 10^3$ | $3.64 \times 10^{-7}$ |
| [241]Am | 26.3 | $1.50 \times 10^2$ | $8.89 \times 10^{-9}$ |
| [241]Am | 59.5 | $2.47 \times 10^3$ | $4.57 \times 10^{-8}$ |

In conclusion the photons doses calculated at the cell entrance are negligible compared to the alpha-particle doses.

# APPENDIX B
## Geometrical parameters
## used for fluence calculations

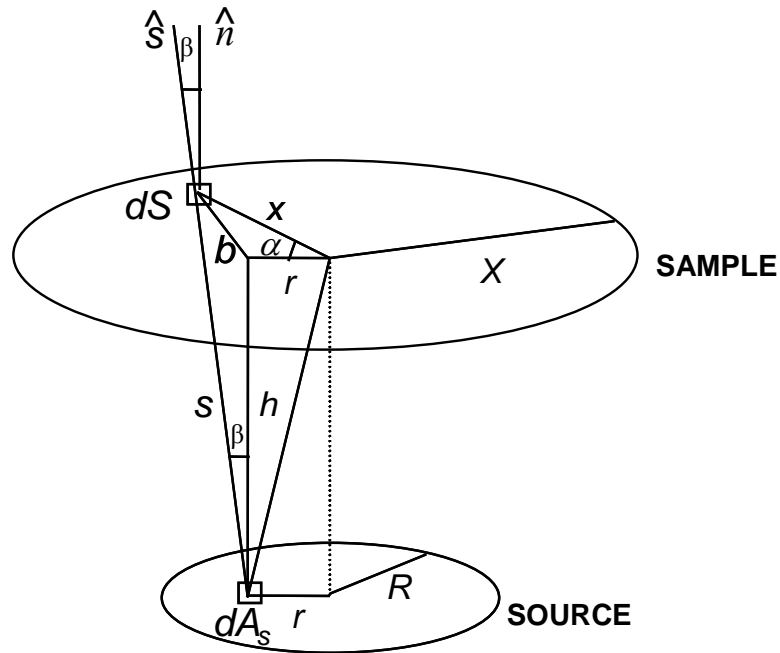Figure B1 shows the geometrical parameters used for fluence calculations.



**Figure B1. Geometrical parameters used for fluence calculations**

The differential particle fluence rate ($d\phi$) at the point of the sample $dS$ is:

$$d\phi = \frac{A}{4\pi^2 R^2} \cdot \frac{dA_s \cos\beta}{s^2}$$

where   $A$ is the activity of the source,
         $R$ is the source radius,
         $dA_s$ is one generic surface element on the source,
         s is the distance between $dA_s$ and $dS$,
         $\beta$ is the angle between the normal to $dS$ and the $s$ direction.
    Since:

$$h = s\,\cos\beta,\ dA_s = r\,dr\,d\alpha$$

$$s = (h^2 + x^2 + r^2 - 2\,r\,x\,\cos\alpha)^{1/2}$$

particle fluence rate $\phi(x)$ as a function of distance x from the centre of the sample was calculated using the relationship:

$$\phi(x) = \frac{A}{4\pi^2 R^2} \int_0^{2\pi} \left( \int_0^R \frac{r \cdot h}{(h^2 + x^2 + r^2 - 2 \cdot r \cdot x \cdot \cos\alpha)^{3/2}}\, dr \right) d\alpha$$

where   $r$ = distance of an arbitrary source point from the source centre
        $h$ = source-to-sample distance
        $x$ = distance of the considered sample point from the sample centre
        $X$ = sample radius
        $\alpha$ = angle between $x$ and the projected $r$

The average particle fluence rate $\bar{\phi}$ is given by:

$$\bar{\phi} = \frac{\int\limits_0^X 2 \cdot \pi \cdot \phi(x) \cdot x \cdot dx}{\pi \cdot X^2}$$

The fluence rate uniformity was evaluated by the ratios of the maximum and minimum fluence rate to its average value:

$$\frac{\phi(x = 0)}{\bar{\phi}}$$

$$\frac{\phi(x = X)}{\bar{\phi}}$$

# APPENDIX C
## Geometrical parameters
## used in simulation by TRIM

To calculate the energy of the alpha particles on the sample, the Monte Carlo code TRIM was used.

The input file given to TRIM includes the information on the particles emitted by the source, that are, for each alpha particle emitted, the energy, the position chosen at random inside a cylinder of $^{244}$Cm or $^{241}$Am atoms with uniform spatial density, and the direction of emission chosen at random within the upper half of the entire solid angle.

$^{244}$Cm decays by emission of a single alpha-particle, with an energy of 5805 keV (emission probability 76.7%) or of 5763 keV (emission probability 23.3%). $^{241}$Am decays by emission of a single alpha-particle, with an energy of 5486 keV (emission probability 85.2%), 5443 keV (emission probability 12.8%), 5388 keV (emission probability 1.4%) or others (emission probability 0.6 %). For both $^{244}$Cm and $^{241}$Am the difference among these energies is negligible for the applications which the irradiator was devoted to. So in the simulation all alpha-particles were emitted with the same energy 5805 keV and 5486 keV for $^{244}$Cm and $^{241}$Am respectively.

Assuming the probability distribution for radiation emission to be isotropic, and neglecting source thickness, the probability of emission $P(\Omega)d\Omega$ in the solid angle $d\Omega$ is simply:

$$P(\Omega)d\Omega = \frac{1}{2\pi}d\Omega \ .$$

Taking into account the relation between $d\Omega$ and the polar $\vartheta$ and azimuthal $\varphi$ angles i.e., $d\Omega = sin(\vartheta)\, d\vartheta\, d\varphi$ :

$$P(\Omega)d\Omega = \frac{1}{2\pi} sin(\vartheta)d\vartheta\, d\varphi = f(\vartheta)d\vartheta \cdot g(\varphi)d\varphi$$

with:

$$f(\vartheta) = sin(\vartheta)$$

$$g(\varphi) = \frac{1}{2\pi}$$

A random direction of the generic particle is then defined by considering two independent random values $a$ and $b$ between 0 and 1 with uniform probability such that:

$$\int_0^{\vartheta} f(\vartheta')d\vartheta' = a$$

$$\int_0^{\varphi} g(\varphi')d\varphi' = b$$

Angles corresponding to a random direction are given by inverting the previous equation:

$$\vartheta = arccos(1 - a)$$

$$\varphi = 2\pi b$$

Each particle has to pass through various materials interposed between the source and the cell monolayer, namely: the gold protective layer, the Mylar® protective cover, the helium gas, and the Mylar® bottom of the Petri dish. The actual path of each alpha particle through these materials depends on its direction of emission.

The geometrical parameters calculated as described above are used by TRIM to evaluate the actual path of gold, helium and Mylar® traversed by each particle, considering its emission angle. The energy spectrum of the particles impinging on the cells was then calculated by considering only the particles with coordinates within the Petri dish. In these calculations the helium density at $37^{\circ}$C was considered, in order to simulate the actual conditions used for the subsequent measurements and for biological experiments.